



PCCP

Functionalized Nona-silicide [Si₉R₃] Zintl Clusters: A New Class of Superhalogens

Journal:	<i>Physical Chemistry Chemical Physics</i>
Manuscript ID	CP-ART-06-2022-002619.R1
Article Type:	Paper
Date Submitted by the Author:	15-Jul-2022
Complete List of Authors:	Sinha, Swapan; Haldia Institute of Technology Jena, Purusottam ; Virginia Commonwealth University, Physics Department Giri, Santanab; Haldia Institute of Technology, School of Applied Sciences

SCHOLARONE™
Manuscripts

ARTICLE

Functionalized Nona-silicide [Si₉R₃] Zintl Clusters: A New Class of Superhalogens

Swapan Sinha,^{a,c} Puru Jena^b and Santanab Giri*^a

Received 00th January 20xx,
Accepted 00th January 20xx

DOI: 10.1039/x0xx00000x

Superatoms, due to their various applications in redox and materials chemistry, have been a major topic of study in cluster science. Superhalogens constitute a special class of superatoms that mimic the chemistry of halogens and serve as building blocks of novel materials such as super and hyper salts, perovskite-based solar cells, solid-state electrolytes, as well as ferroelectric materials. These applications have led to a constant search for new class of superhalogens. In this study, using density functional theory, we show that recently synthesized [Si₉{Si('Bu)₂H₃}₃] and [Si₉{Si(TMS)₃}₃] Zintl clusters not only behave like halogens but also when functionalized with suitable ligands exhibit superhalogen characteristics. Frontier molecular orbitals (FMOs) analyses give insights into the electron-acceptor nature of the Zintl clusters. Additional bonding techniques such as energy density at bond critical point (BCP) and adaptive natural density partitioning (AdNDP) gives complementary information about the nature of bonding in Si-based Zintl clusters. The potential of these Zintl clusters in the synthesis of new electrolytes in Li-ion batteries is also investigated.

INTRODUCTION

The origin of Zintl chemistry dates back to 1891 when a French scientist, Alexandre Joannis mixed a pure solid alkali metal like sodium (Na) with the main group element lead (Pb) in liquid ammonia and observed a deep green solution^{1, 2}. At the time, no one knew what was actually happening in this particular reaction, although later many speculated that when an alkali metal is mixed with main group elements, it forms a highly reduceable chemical compound that mainly contains these main group elements. It was not until 1931 when Zintl and co-workers³ confirmed the deep green solution to be Na₄Pb₉. Here, the Pb₉⁴⁻ cluster is surrounded by alkali metal atoms; hence, Na₄Pb₉ came to be known as the Zintl phase⁴ and Pb₉⁴⁻-like multi-anionic polyatomic clusters as Zintl clusters. The basic unit of the Zintl cluster can be written as X_Nⁿ⁻ where X = Si, Ge, Sn, Pb, As, Sb, Bi; N = number of atoms and n is the number of negative charges. Among these, germanium based Zintl clusters are well known from both experimental and theoretical points of view, and their structural characteristics, stability, and functionalization have been studied⁵⁻¹².

However, Zintl clusters based on Si are not common, even though Si and Ge belong to the same group of elements. Although solid Zintl phase of A₄Si₄ [where A = alkali metal]

exists, A₄Si₉ has not been discovered. Sevov et al.¹³ had isolated compounds like Rb₁₂Si₁₇, where both Si₄⁴⁻ and Si₉⁴⁻ moieties exist in a 2:1 ratio¹⁴. Functionalization of Zintl clusters is a recent trend in cluster chemistry. For example, functionalization¹⁵⁻²³ of nona-germanium based Zintl clusters is well established from its well-known Zintl phase (K₄Ge₉), but due to the absence of nonasilicide, functionalization of Zintl phase (A₄Si₉) has been challenging for an experimental chemist. Recently, the mono- and di-protonated nonasilicides (HSi₉³⁻, H₂Si₉²⁻) were obtained from the A₁₂Si₁₇ [A = K, Rb] Zintl phase^{24, 25}. In addition, analogous to protonation, silylation and stannylation have been carried out by Fassler et al.^{26, 27} and Zintl clusters [Si₉R₂]²⁻, [Si₉R₃]⁻ [where R = SiH('Bu)₃, SnCy₃, Si(TMS)₃] have been produced.

In this paper, we study silicon-based organo-Zintl clusters (Si₉R₃) and find some of these to have superhalogen character, i.e., their electron affinities (EA) are higher than that of halogens, e.g., chlorine (Cl) atom with EA = 3.6 eV. The existence of superhalogens^{28, 29} was first predicted by Gutsev and Boldyrev in 1981 and later experimentally confirmed by Wang et al.^{30, 31}. Although several types of superhalogens are now available in the literature³²⁻³⁸, silicon-based Zintl superhalogens have not yet been reported. Here, we show that functionalized nonasilicide Zintl cluster can be a potential superhalogen candidate, having oxidizing properties. It is well known that the Si₉⁴⁻ has a reducing character i.e., it releases electrons and transforms into Si₉³⁻ and Si₉²⁻³⁹. Thus, it is a challenging task to design a nonasilicide Zintl cluster having oxidizing/superhalogen character.

Note that electronegative ligands such as -CF₃, -CN, -BO, -NO₂ etc can be used to functionalize clusters to enhance their

^a School of Applied Science and Humanities, Haldia Institute of Technology, Haldia, India 721657,

^b Physics Department, Virginia Commonwealth University, Richmond, Virginia 23284, United States.

^c Maulana Abul Kalam Azad University of Technology, Haringhata, 741249, India

* Email: sgiri.chem@hithaldia.in

† Electronic Supplementary Information (ESI) available: [details of any supplementary information available should be included here]. See DOI: 10.1039/x0xx00000x

electron affinities and hence create superhalogens^{33, 40-42}. From the previous study, it has been established that functionalized germanium Zintl cluster Ge_9R_3 (R = $-\text{CF}_3$, $-\text{CN}$, $-\text{NO}_2$ group) act as superhalogen³³. Further, clusters like icosahedral dodecaborate anion, $\text{B}_{12}\text{H}_{12}^{2-}$ is found to be a more stable dianion when $-\text{H}$ is replaced by $-\text{CN}$ i.e., $\text{B}_{12}(\text{CN})_{12}^{2-}$ ^{40, 41, 43}. In this work, we have also taken these electron-withdrawing ligands to see if Si_9R_3 (where R = $-\text{CF}_3$, $-\text{CN}$, $-\text{NO}_2$) clusters could be superhalogens. Note that Si_9^{4-} contains 40 electrons [(4 $e^- \times 9 = 36$ electrons of Si) + (4 extra electrons) = 40] and, according to the jellium model, could be very stable. We hypothesized that a cluster like Si_9R_3 (where R = $-\text{CF}_3$, $-\text{CN}$, $-\text{NO}_2$) would contain 39 electrons and hence could mimic the properties of halogens as one extra electron is needed to stabilize $[\text{Si}_9\text{R}_3]$. The question remains: would Si_9R_3 have a high electron affinity? We set out to see if this indeed is the case.

COMPUTATIONAL DETAILS

First, the ground state geometry of bare Si_9^{4-} was obtained by using density functional theory with B3LYP⁴⁴ functional and two different basis sets [SDD and 6-311+G(d,p)]^{45, 46}. Vibrational frequency analyses were performed at the same level of computation. The results suggest that the bare silicon cluster resides on the local minimum of the potential energy surface. Next, we computed the geometry of experimentally observed nonasilicide clusters $[\text{Si}_9\{\text{Si}(\text{tBu})_2\text{H}\}_3]_3$, $[\text{Si}_9\{\text{Si}(\text{TMS})_3\}_3]$. As these are large structures, we used only the SDD basis set. For other functionalized Si_9R_3 clusters, we used the 6-311+G(d,p) basis sets. The possible superhalogen nature of these clusters is studied by calculating the electron affinity (EA) and vertical detachment energy (VDE). The former is the energy difference between the ground states of both the anion and the neutral while the latter is the energy difference between the ground state of the anion and the corresponding neutral having the anion geometry. To get more accurate energy values and to validate our computational procedure, we further used large basis sets like def2tzvp and MP2-level of theory. The nature of bonding between the ligand and the Zintl cluster core is studied using Bader's Quantum theory of atoms in the molecule (QTAIM) approach^{47, 48}. This is illustrated by the gradient map of the electron density with bond paths and bond critical points. All calculations are done using *Gaussian 09* and *Multifn* program packages^{49, 50}.

RESULTS AND DISCUSSION

We begin with the geometry of the Si_9^{4-} core cluster, which is then functionalized to study the possibility of creating new superhalogens. The calculated geometry given in Fig. 1 is found to have a D_{3h} point group symmetry. The NBO charge analysis in Fig. 1 shows that the Si atoms situated at each of the three capped positions (3,6,8) carry charges of -0.57, which are more negative than that on the other Si atoms. This indicates that capped sites are ideal for ligand functionalization, which is consistent with experiment¹⁸. The

important bond distances are also given in this figure. The distances from the capped Si (3, 6, 8) connected to the nearest Si atoms (1,2,4,5,7,9) are similar, namely, 2.52 Å. The distances between Si atoms marked 1-5, 2-4, 9-7 are also the same, namely 2.54 Å. Small changes in bond distances are observed for atoms marked 1-2 and 4-5. It is noticed that the Si-Si bond length in Si_9^{4-} cluster is notably higher than the Si-Si bond lengths in the well-known silicene [buckled state (2.247 Å) and flat state (2.226 Å)] and other silicon-based compounds^{51, 52}. This is due to the negative charge on the Si atom in Si_9^{4-} cluster which results in the increased bond length.

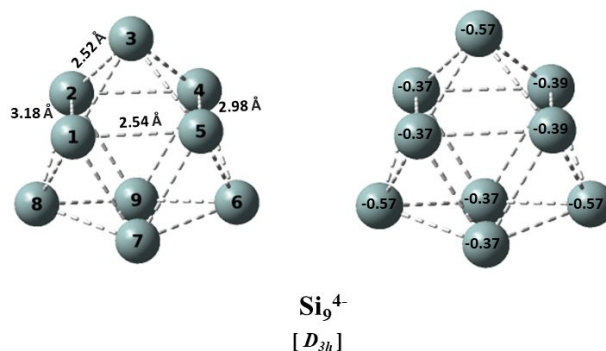


Fig. 1 Ground-state geometry of Si_9^{4-} with NBO charges on each silicon atom.

The cluster contains 40 electrons, sufficient to close the jellium electronic shells. The electronic configuration of Si_9^{4-} according to jellium shell model is $1S^2 1P^6 1D^{10} 2S^2 1F^4 2P^2 1F^6 2P^2 1F^4 2P^2$. The schematic representation of jellium model is given in

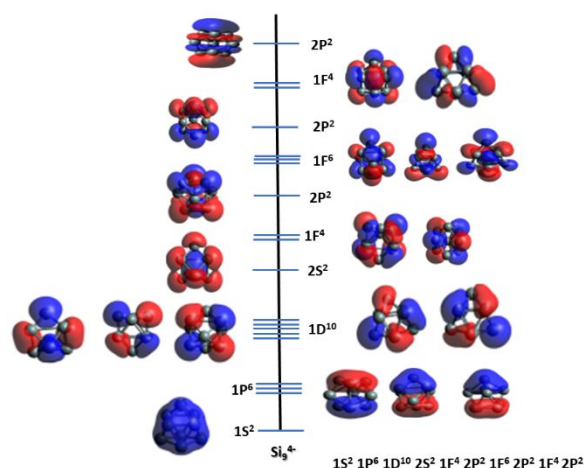


Fig 2.

Fig. 2 Jellium electronic shell configuration of Si_9^{4-} .

To study the superhalogen properties of Si-based Zintl clusters, we start with the experimentally synthesized cluster $[\text{Si}_9\{\text{Si}(\text{tBu})_2\text{H}\}_3]_3$, $[\text{Si}_9\{\text{Si}(\text{TMS})_3\}_3]$. The optimized geometries of these anionic clusters are given in Fig. 3. The calculated structural parameters match well with the crystallographic data.

The anions contain 40 electrons ($4 \times 9 = 36$ electrons on Si atoms, $1 \times 3 = 3$ electrons on ligands, and 1 electron due to the added negative charge). The stability of these anions can be explained in terms of the jellium electronic shell closure model. The schematic representation of jellium model along with electronic configuration of $[\text{Si}_9\{\text{Si}(\text{TMS})_3\}_3]^-$ is given in Fig. 4 and rest are given in the supporting information Fig S1-S2. The electronic configuration of $[\text{Si}_9\{\text{Si}(\text{TMS})_3\}_3]^-$ according to jellium electronic shell closure model is $1\text{S}^2 1\text{P}^6 1\text{D}^8 2\text{P}^4 1\text{D}^2 2\text{P}^2 1\text{F}^{10} 2\text{S}^2 1\text{F}^4$.

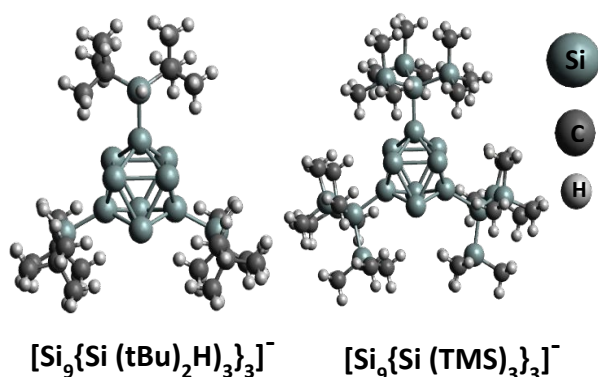


Fig. 3 Ground state geometries of $[\text{Si}_9\{\text{Si}(\text{tBu})_2\text{H}\}_3]^-$ and $[\text{Si}_9\{\text{Si}(\text{TMS})_3\}_3]^-$.

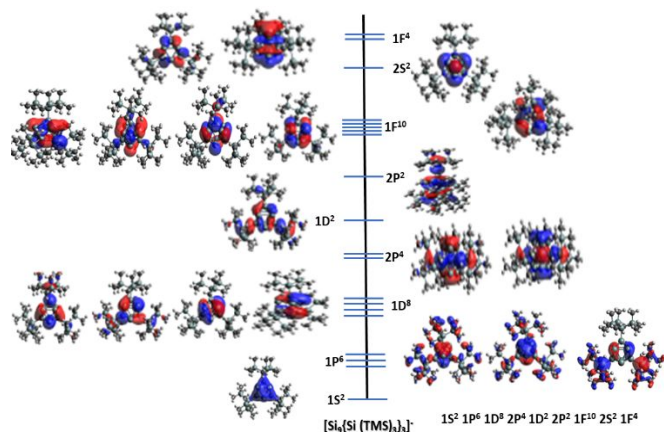


Fig. 4 Jellium electronic shell configuration of the $[\text{Si}_9\{\text{Si}(\text{TMS})_3\}_3]^-$.

The calculated vertical detachment energies (VDE) of these clusters are given in Table 1. They lie in the range of 3.4–3.6 eV, which are very similar to the electron affinities of halogens ($\text{EA} = 3.06 - 3.61$ eV). Thus, these Si-based Zintl clusters mimic the chemistry of halogens and ligand plays an important role in this regard. We wondered if a proper choice of ligands could lead to a Si-based Zintl superhalogen cluster.

Table 1: Experimental (exp) and calculated (cal) Si-Si exo-bond length (in Å), calculated vertical detachment energy (VDE) of experimentally synthesized Zintl cluster using B3LYP/SDD, B3LYP/6-311+G (d, p) level of theory.

Cluster	Average (exp) Exo Si-Si bond length (Å)	Average (cal) Exo Si-Si bond length (Å)		Vertical detachment energy (eV)	
		B3LYP /SDD	B3LYP /6-311+G (d, p)	B3LYP /SDD	B3LYP/6-311+G (d, p)
$\text{Si}_9\{\text{Si}(\text{tBu})_2\text{H}\}_3$	2.36	2.39	2.36	3.51	3.55

Superhalogen Character

We designed four Zintl clusters functionalized with $-\text{CH}_3$, $-\text{CF}_3$, $-\text{CN}$, and $-\text{NO}_2$ ligands. Here, $-\text{CH}_3$ is as an electron-donating group while $-\text{CF}_3$, $-\text{CN}$, and $-\text{NO}_2$ are electron-withdrawing groups. Corresponding optimized geometries of $[\text{Si}_9(\text{CH}_3)_3]^-$, $[\text{Si}_9(\text{CF}_3)_3]^-$, $[\text{Si}_9(\text{CN})_3]^-$, and $[\text{Si}_9(\text{NO}_2)_3]^-$ anions are given in Fig. 5. To see the changes in the core structure upon ligand substitution, we compare the bond distances of Si atoms between the naked (Si_9^{4-}) and the ligated clusters (Si_9R_3^-). The bond distances between the capped Si (3, 6, 8) connected to the nearest Si atoms (1, 2, 4, 5, 7, 9) are reduced by 0.09 Å. The other bond distances are found to be marginally increased compared to those in the Si_9^{4-} cluster. No marked change in the geometry of the core is seen and this observation is independent of the nature of the ligand.

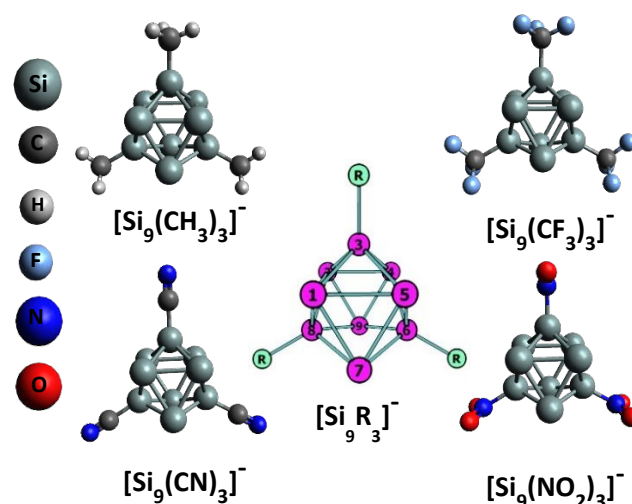


Fig. 5 Ground state anionic geometries of $[\text{Si}_9(\text{CH}_3)_3]^-$, $[\text{Si}_9(\text{CF}_3)_3]^-$, $[\text{Si}_9(\text{CN})_3]^-$ and $[\text{Si}_9(\text{NO}_2)_3]^-$. Each atom is represented by different colours as indicated.

Table 2: Calculated vertical detachment energy (VDE) and electron affinity (EA) [within brackets] of Zintl systems at the B3LYP/6-311+G (d, p), MP2/6-311+G (d, p), B3LYP/def2tzvp level of theory.

Cluster/ligand	VDE of individual ligands	Vertical Detachment Energy (Electron Affinity) in eV unit		
		B3LYP/6-311+G (d, p)	B3LYP/def2tzvp	MP2/6-311+G (d, p)
$\text{Si}_9(\text{CH}_3)_3/\text{CH}_3$	-0.078	3.101 (2.830)	2.958	3.008
$\text{Si}_9(\text{CF}_3)_3/\text{CF}_3$	-0.889	4.349 (4.039)	4.137	4.199
$\text{Si}_9(\text{CN})_3/\text{CN}$	4.076	4.522 (4.287)	4.382	4.711
$\text{Si}_9(\text{NO}_2)_3/\text{NO}_2$	2.956	4.697 (4.436)	4.494	4.339

To study their superhalogen character, we calculated the vertical detachment energies (VDE). The results are given in Table 2. Note that the VDE values range from 3 eV to 4.7 eV. The results are insensitive to different basis sets and treatment of exchange-correlation potential. With the exception of $[\text{Si}_9(\text{CH}_3)_3]$ where $-\text{CH}_3$ is an electron-donating ligand, the remaining Zintl clusters are all superhalogens, with the VDE values of $[\text{Si}_9(\text{CF}_3)_3]$, $[\text{Si}_9(\text{CN})_3]$, and $[\text{Si}_9(\text{NO}_2)_3]$ clusters being 4.349, 4.522 and 4.697 eV, respectively, at the B3LYP/6-311+G (d, p) level of theory. We have also calculated the electron affinity (EA) of these modelled clusters using the same level of theory [see Table 2 value within brackets]. Note that the VDE and EA values are rather close to each other reflecting that there is little change in the geometry when an electron is detached from the anion. All the EA values are larger than 4 eV and have a similar trend as the VDEs. As VDE and EA values are higher than that of the halogen atoms, the corresponding clusters can be considered as superhalogens. The reason is that the electron-withdrawing ligands withdraw electrons from the Zintl core, making it electron-deficient and hence leading to high VDE values.

Frontier Molecular Orbitals (FMOs) Analysis

To understand the origin of the superhalogen behaviour of the Zintl clusters, we examine their electronic structures, beginning with the FMOs analysis in Fig. 6. The extra electron is expected to attach to the singly occupied molecular orbital (SOMO). Thus, it can reveal the variation of the VDE in Zintl systems. We see that the SOMO energies of $[\text{Si}_9(\text{CF}_3)_3]$, $[\text{Si}_9(\text{CN})_3]$, and $[\text{Si}_9(\text{NO}_2)_3]$ clusters are lower than that of the $[\text{Si}_9(\text{CH}_3)_3]$ cluster, which indicates that the electron-withdrawing ligands are lowering the SOMO energy levels, making the Zintl clusters better electron acceptors.

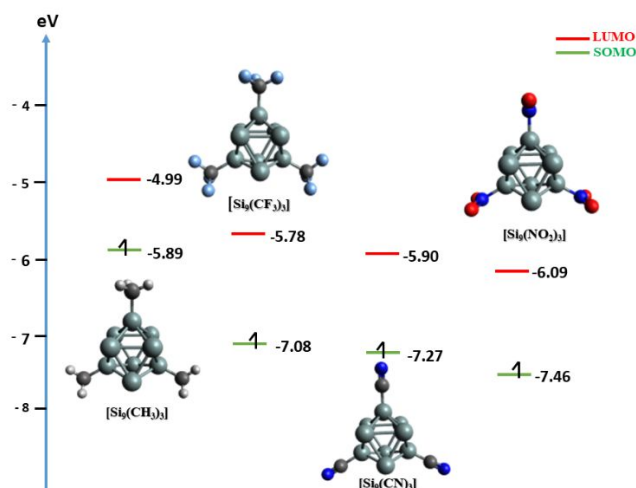


Fig. 6 Molecular orbital energy diagram near the SOMO, LUMO (in eV) of the studied Zintl clusters. The color code for different coloured atoms are same as Figure 5.

Bonding Analysis

Next, we study the bonding characteristics of the studied clusters by analyzing the contour gradient map of the electron density along with the bond path, bond critical points, Adaptive Natural Density Partitioning (AdNDP) analysis, and electron localization function (ELF) study.

Gradient map of electron density with bond paths and bond critical points

To determine if the bonding between the ligands and the Si_9 core is ionic or covalent, we first study the gradient map of the electron density with bond paths and bond critical points in Fig. 7 and Fig. 8, respectively. The brown solid lines indicate bond pathways, and the solid bold blue lines that separate the atomic nuclei show zero-flux molecular plane surfaces. Bond critical points (3, -1) which are represented by the light blue spheres are points where the bond path and zero-flux surfaces cross. Ring critical points (3, +1) and cage critical points (3, +3) are represented in orange and green spheres, respectively. Here, a negative value of the Laplacian ($\nabla^2\rho(r) < 0$) at BCP corresponds to the covalent nature of the bond, while a positive value of the Laplacian ($\nabla^2\rho(r) > 0$) shows the non-covalent (ionic/polar) nature of the bond. Like Laplacian electron density, energy density (H) values also tell us about the nature of the bond, where negative and positive values of energy density (H/BCP) correspond to covalent and ionic nature, respectively.

From Fig. 7, we see that the BCPs (3, -1) between Si-Si in $[\text{Si}_9\{\text{Si}(\text{tBu})_2\text{H}\}_3]^-$ and $[\text{Si}_9\{\text{Si}(\text{TMS})_3\}_3]^-$ suggest the existence of a chemical bond between Zintl core and the ligands. The values of the Laplacian of electron density ($\nabla^2\rho$) and energy density (H) values at BCP (3, -1) between three Si-Si bonds are given in Table S1. The Laplacian of electron density ($\nabla^2\rho$) and energy density (H) values at BCP (3, -1) between three Si-Si bonds are negative, which indicates the covalent nature of the Si-Si bond in these systems.

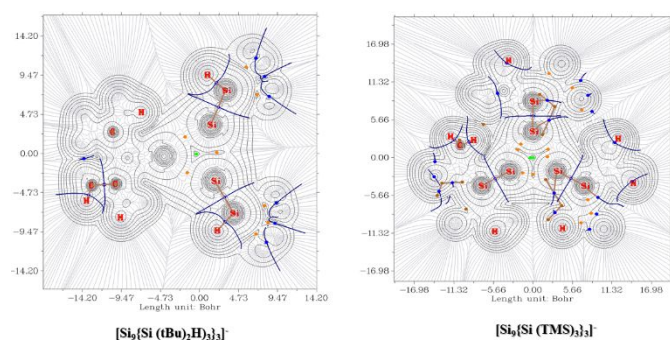


Fig. 7 Contour plot of the Laplacian of the electron density along with bond path and bond critical points of $[\text{Si}_9\{\text{Si}(\text{'Bu})_2\text{H}\}_3]^{3-}$ and $[\text{Si}_9\{\text{Si}(\text{TMS})\}_3]^{3-}$ on the XY plane.

In $[\text{Si}_9(\text{CF}_3)_3]^-$, $[\text{Si}_9(\text{CN})_3]^-$ and $[\text{Si}_9(\text{NO}_2)_3]^-$ clusters, we also observe the BCP (3, -1) between the Zintl core and the ligands. The corresponding Laplacian ($\nabla^2\rho$) and energy density (H) values at BCP (3, -1) between core and ligands are positive and negative, respectively. The results are given in Table S2 and indicate the bonding to be between covalent and ionic.

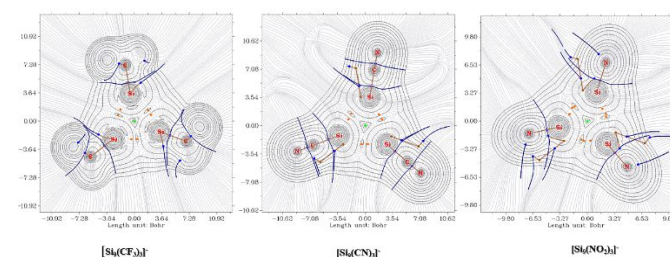


Fig. 8 Contour plot of the Laplacian of the electron density along with bond path and bond critical points of $[\text{Si}_9(\text{CF}_3)_3]^-$, $[\text{Si}_9(\text{CN})_3]^-$ and $[\text{Si}_9(\text{NO}_2)_3]^-$ on the XY plane.

AdNDP analysis

To overcome the limitation of the Laplacian ($\nabla^2\rho$) and energy density (H) rules in describing the nature of bonding, we further carry out the adaptive natural density partitioning (AdNDP)⁵³⁻⁵⁸ analysis using the Multiwfn program⁵⁰. Based on the NBO (Natural Bonding Orbital) theory, AdNDP is a newly developed computational algorithm, which can entirely explain the bonding nature of the molecules, i.e. N-centre-2 electron bond [Nc-2e bond] (where N= number of centers). Thus, the AdNDP analysis tells us about how many centers are involved to make a two-electron bond.

For the experimentally realized systems, we found 2c-2e bond with high 1.98|e| occupation numbers, which is depicted in Fig. 9. The high occupancy indicates that both the core and the ligands share one electron and make 2c-2e bond, which confirms the covalent nature of the bond between the silicon cluster and the ligands.

In the clusters we have designed, 2c-2e bond exists between the substituted Si atom and central atom of the ligands with 1.99 |e| occupation number. The 2c-2e bond AdNDP of $[\text{Si}_9(\text{CF}_3)_3]^-$ is given in Fig. 10 and others are given in the Supporting Information Fig. S3. The high occupation number

indicates that both the Zintl core and ligands are sharing electrons to make a 2c-2e bond.

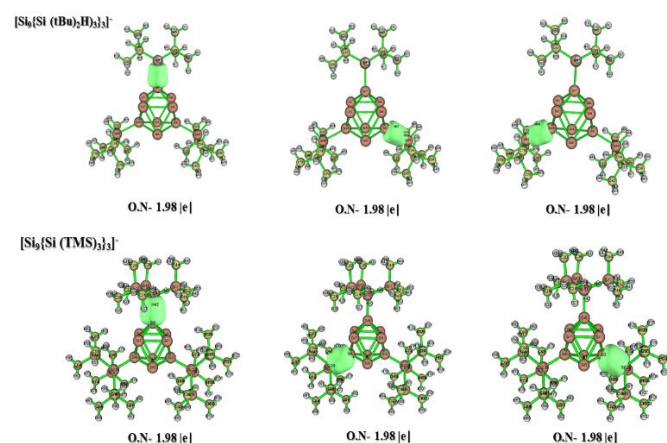


Fig. 9 AdNDP study of the $[\text{Si}_9\{\text{Si}(\text{'Bu})_2\text{H}\}_3]^{3-}$ and $[\text{Si}_9\{\text{Si}(\text{TMS})\}_3]^{3-}$ with occupation number of 1.98 |e|.

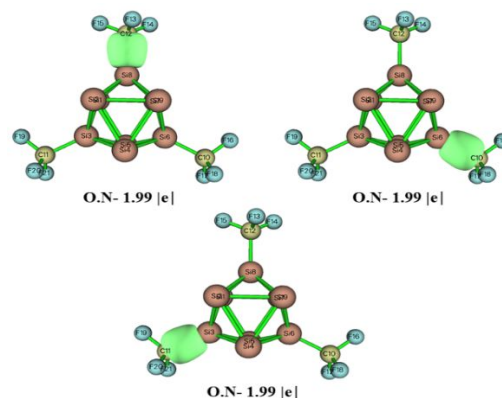


Fig. 10 AdNDP study of the $[\text{Si}_9(\text{CF}_3)_3]^-$ with occupation number of 1.99 |e|.

In-depth bonding analyses of Si_9 cluster is further illustrated by the electron localization function (ELF) study⁵⁹. The corresponding results are given in Fig. 11 and Fig S4. It clearly indicates that there is a strong electron localization between Si_9 core and the Ligand, which confirms the covalent nature of bond between Si_9 core and the ligand.

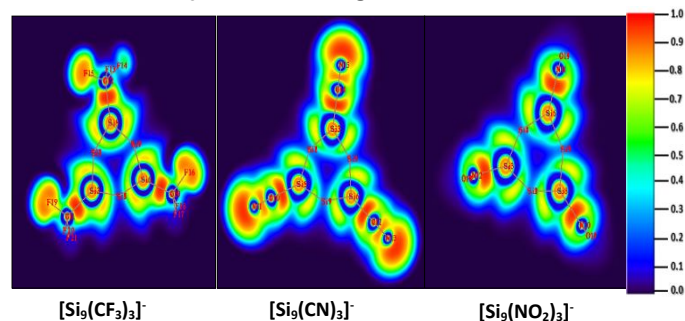


Fig. 11 Cut of plane ELF plot of $[\text{Si}_9(\text{CF}_3)_3]^-$, $[\text{Si}_9(\text{CN})_3]^-$ and $[\text{Si}_9(\text{NO}_2)_3]^-$.

Possible electrolytes in Li-ion batteries

As silicon-based Zintl clusters studied here are stable as a monoanion, we study their potential to serve as negative ion components of electrolytes in Li-ion batteries. From previous studies³², it was predicted and later confirmed^{60, 61} that $\text{CB}_{11}\text{H}_{12}^-$ is an effective halogen-free electrolyte for Li-ion batteries. One of the relevant quantities that determine the effectiveness of an electrolyte is the energy it takes to dissociate the electrolyte salt into individual ions. Thus, we calculated the Li-ion binding energy in the Si-based Zintl clusters. The ground state geometries of these systems are given in the Supporting Information (Fig. S5, S6). The corresponding binding energies and molar volumes of individual systems are given in Table 3. The Li-ion binding energy of $\text{Si}_9\text{R}_3\text{Li}$ is calculated using the formula $\Delta E_{\text{Li}^+} = \{E(\text{Si}_9\text{R}_3\text{Li})\} - \{E(\text{Si}_9\text{R}_3^-) + E(\text{Li}^+)\}$.

Note that the Li-ion binding energies of the synthesized $[\text{Si}_9\{\text{Si}(\text{TMS})_3\}_3]^-$, $[\text{Si}_9\{\text{Si}(\text{tBu})_2\text{H}\}_3]^-$ and our modelled systems are lower than that of $\text{LiCB}_{11}\text{H}_{12}$, showing the potential of the Si-based Zintl anions as building blocks of electrolytes. We have also calculated the Li-binding energy in solvent phase. As carbonates are commonly used as organic solvent in Li-ion batteries, we have considered dimethyl carbonate (DMC) as a solvent. The calculated solvent phase Li-ion binding energy i.e., ΔE_{Li^+} (eV) values are also given in Table 3. The negative binding energy values suggest that the Li loosely binds with Si clusters which results easy Li-ion conduction.

Table 3: The calculated Li-ion binding energy i.e., ΔE_{Li^+} (eV) of earlier reported and our studied systems.

Anions	Molar Volume ($\text{cm}^3 \text{mol}^{-1}$)	ΔE_{Li^+} (in eV)			
		B3LYP/SDD	B3LYP/6-311+G(d,p)	wB97XD/6-311+G(d,p)	wB97XD/6-311+G(d,p) in solvent phase (DMC)
PF_6 (reported)	46.62	-	-	-5.73	-
AsF_6 (reported)	58.17	-	-	-5.65	-
$\text{CB}_{11}\text{H}_{12}$ (reported)	126.78	-	-	-5.08	-
$[\text{Si}_9\{\text{Si}(\text{TMS})_3\}_3]^-$	790.96	-5.22	-5.21	-5.22	-2.11
$[\text{Si}_9\{\text{Si}(\text{tBu})_2\text{H}\}_3]^-$	617.74	-5.31	-5.27	-5.22	-1.10
$[\text{Si}_9(\text{CF}_3)_3]^-$	250.01	-4.86	-4.86	-4.82	-1.02
$[\text{Si}_9(\text{CN})_3]^-$	287.16	-4.21	-4.35	-4.30	-0.87
$[\text{Si}_9(\text{NO}_2)_3]^-$	250.51	-4.01	-4.22	-4.15	-0.75

CONCLUSIONS

Zintl ions composed of Ge and Pb are common but those based on the same group Si are rare. Recent synthesis of Zintl ions based on Si such as Si_9R_3 [R= Si (TMS)₃, Si (tBu)₂H]₃] motivated us to study if these ions with a suitable choice of ligands could be candidates for superhalogens. Using density functional theory (DFT) with hybrid functional for exchange-correlation potential and Gaussian basis sets, we found that although the electron affinities of the synthesized Zintl ions are close to that of the halogens, they are not superhalogens. To study the effect of ligands on the electronegative properties of Si-based Zintl ions, we chose two different kinds of ligands - CH_3 that donates electrons, and $-\text{CF}_3$, $-\text{CN}$, $-\text{NO}_2$ ligands that accept electrons. Functionalized nona-silicide Zintl clusters (Si_9R_3) [R= $-\text{CF}_3$, $-\text{CN}$, $-\text{NO}_2$] are all found to have vertical detachment energies and electron affinities above 4 eV and hence are all superhalogens. Electronic structure analysis based on HOMO and LUMO orbitals, bond paths, bond critical points, and AdNDP showed that the bonding between the ligand and the Si_9^{4-} core is predominantly covalent. Further,

both the ligand and the core share one electron to make a 2c-2e bond. The potential of these Si-based Zintl anions in forming electrolytes in Li-ion batteries is studied by calculating the energy to dissociate $\text{Li}(\text{Si}_9\text{R}_3)$ [R= $-\text{CF}_3$, $-\text{CN}$, $-\text{NO}_2$] into Li cations and Zintl anions. The results show that these binding energies are less than that in $\text{LiCB}_{11}\text{H}_{12}$ which is already proven to be a good electrolyte for Li-ion batteries. Our study expands the scope of superhalogens and, hence, their potential for applications.

Author Contributions

The manuscript was written through the contributions of all authors. All authors have given approval to the final version of the manuscript.

Conflicts of interest

"There are no conflicts to declare".

Acknowledgements

This work is supported by the Department of Science and Technology INSPIRE award no. IFA14-CH-151, SERB projects CRG/2019/001125, and SB/FT/CS-002/2014, Government of India. P. J. acknowledges partial support by the U.S. Department of Energy, Office of Basic Energy Sciences, Division of Materials Sciences and Engineering under Award DE-FG02-96ER45579.

Notes and references

1. M. Joannis, *CR Hebd. Seances Acad. Sci*, 1891, **113**, 795-798.
2. Y. Heider and D. Scheschkewitz, *Chemical Reviews*, 2021, **121**, 9674-9718.
3. E. Zintl and A. Harder, *Zeitschrift für Physikalische Chemie*, 1931, **154A**, 47-91.
4. E. Zintl and W. Dullenkopf, *Zeitschrift für Physikalische Chemie*, 1932, **16B**, 183-194.
5. D. J. Chapman and S. C. Sevov, *Inorganic Chemistry*, 2008, **47**, 6009-6013.
6. C. Liu and Z.-M. Sun, *Coordination Chemistry Reviews*, 2019, **382**, 32-56.
7. S. Giri, G. N. Reddy and P. Jena, *The Journal of Physical Chemistry Letters*, 2016, **7**, 800-805.
8. M. W. Hull and S. C. Sevov, *Inorganic Chemistry*, 2007, **46**, 10953-10955.
9. D. Xue, D. Wu, Z. Chen, Y. Li, W. Sun, J. Liu and Z. Li, *Inorg. Chem.*, 2021, **60**, 3196.
10. N. V. Tkachenko and A. I. Boldyrev, *Chemical Science*, 2019, **10**, 5761-5765.
11. J. Roziere, A. Seigneurin, C. Belin and A. Michalowicz, *Inorganic Chemistry*, 1985, **24**, 3710-3712.
12. P. Andre Clayborne and H. Häkkinen, *Physical Chemistry Chemical Physics*, 2012, **14**, 9311-9316.
13. V. Quéneau, E. Todorov and S. C. Sevov, *Journal of the American Chemical Society*, 1998, **120**, 3263-3264.
14. H. G. von Schnering, M. Somer, M. Kaupp, W. Carrillo-Cabrera, M. Baitinger, A. Schmeding and Y. Grin, *Angewandte Chemie International Edition*, 1998, **37**, 2359-2361.
15. R. Inostroza-Rivera, R. Parida, S. Nambiar and S. Giri, *The Journal of Physical Chemistry A*, 2021, **125**, 2751-2758.
16. S. Frischhut, M. M. Bentlohner, W. Klein and T. F. Fässler, *Inorganic Chemistry*, 2017, **56**, 10691-10698.
17. L. G. Perla and S. C. Sevov, *Journal of the American Chemical Society*, 2016, **138**, 9795-9798.
18. F. Li and S. C. Sevov, *Inorganic Chemistry*, 2012, **51**, 2706-2708.
19. O. Kysliak and A. Schnepf, *Dalton Transactions*, 2016, **45**, 2404-2408.
20. R. Báez-Grez, J. Garza, A. Vásquez-Espinal, E. Osorio, W. A. Rabanal-León, O. Yañez and W. Tiznado, *Inorganic Chemistry*, 2019, **58**, 10057-10064.
21. D. Rios and S. C. Sevov, *Inorganic Chemistry*, 2010, **49**, 6396-6398.
22. L. G. Perla, A. Muñoz-Castro and S. C. Sevov, *Journal of the American Chemical Society*, 2017, **139**, 15176-15181.
23. C. Wallach, F. S. Geitner, A. J. Karttunen and T. F. Fässler, *Angewandte Chemie International Edition*, 2021, **60**, 2648-2653.
24. T. Henneberger, W. Klein and T. F. Fässler, *Zeitschrift für anorganische und allgemeine Chemie*, 2018, **644**, 1018-1027.
25. L. J. Schiegerl, A. J. Karttunen, J. Tillmann, S. Geier, G. Raudaschl-Sieber, M. Waibel and T. F. Fässler, *Angewandte Chemie*, 2018, **130**, 13132-13137.
26. L. J. Schiegerl, A. J. Karttunen, W. Klein and T. F. Fässler, *Chemistry – A European Journal*, 2018, **24**, 19171-19174.
27. L. J. Schiegerl, A. J. Karttunen, W. Klein and T. F. Fässler, *Chemical science*, 2019, **10**, 9130-9139.
28. G. L. Gutsev and A. I. Boldyrev, *Chemical Physics*, 1981, **56**, 277-283.
29. G. L. e. Gutsev and A. I. Boldyrev, *Russian Chemical Reviews*, 1987, **56**, 519.
30. X.-B. Wang, C.-F. Ding, L.-S. Wang, A. I. Boldyrev and J. Simons, *The Journal of Chemical Physics*, 1999, **110**, 4763-4771.
31. M. M. Wu, H. Wang, Y. J. Ko, Q. Wang, Q. Sun, B. Kiran, A. K. Kandalam, K. H. Bowen and P. Jena, *Angewandte Chemie International Edition*, 2011, **50**, 2568-2572.
32. S. Giri, S. Behera and P. Jena, *Angew. Chem., Int. Ed.*, 2014, **53**, 13916.
33. G. N. Reddy, R. Parida and S. Giri, *Chemical Communications*, 2017, **53**, 13229-13232.
34. D. Samanta, *The Journal of Physical Chemistry Letters*, 2014, **5**, 3151-3156.
35. S. Smuczyńska and P. Skurski, *Inorganic Chemistry*, 2009, **48**, 10231-10238.

36. Y. Jiang, Z. Li, J. Zhang and Z. Wang, *The Journal of Physical Chemistry C*, 2020, **124**, 2131-2136.
37. A. Omidvar, *Inorganic Chemistry*, 2018, **57**, 9335-9347.
38. P. Koirala, M. Willis, B. Kiran, A. K. Kandalam and P. Jena, *The Journal of Physical Chemistry C*, 2010, **114**, 16018-16024.
39. S. Joseph, C. Suchentrunk, F. Kraus and N. Korber, *European Journal of Inorganic Chemistry*, 2009, **2009**, 4641-4647.
40. H. Zhao, J. Zhou and P. Jena, *Angewandte Chemie International Edition*, 2016, **55**, 3704-3708.
41. M. Mayer, V. van Lessen, M. Rohdenburg, G.-L. Hou, Z. Yang, M. Exner Rüdiger, E. Aprà, A. Azov Vladimir, S. Grabowsky, S. Xantheas Sotiris, R. Asmis Knut, X.-B. Wang, C. Jenne and J. Warneke, *Proceedings of the National Academy of Sciences*, 2019, **116**, 8167-8172.
42. H.-J. Zhai, Q. Chen, H. Bai, S.-D. Li and L.-S. Wang, *Accounts of Chemical Research*, 2014, **47**, 2435-2445.
43. A. A. Kamin and M. A. Juhasz, *Inorganic Chemistry*, 2020, **59**, 189-192.
44. C. Lee, W. Yang and R. G. Parr, *Phys. Rev. B: Condens. Matter Mater. Phys.*, 1988, **37**, 785.
45. R. Krishnan, J. S. Binkley, R. Seeger and J. A. Pople, *The Journal of Chemical Physics*, 1980, **72**, 650-654.
46. J. A. Pople, P. M. W. Gill and B. G. Johnson, *Chemical Physics Letters*, 1992, **199**, 557-560.
47. R. F. W. Bader, *The Journal of Physical Chemistry A*, 1998, **102**, 7314-7323.
48. R. F. W. Bader, *Atoms in Molecules: A Quantum Theory*, 1990.
49. M. J. Frisch, <http://www.gaussian.com/>, 2009.
50. T. Lu and F. Chen, *J. Comput. Chem.*, 2012, **33**, 580.
51. Y.-X. Yu, *The Journal of Physical Chemistry C*, 2019, **123**, 205-213.
52. A. Molle, C. Grazianetti, L. Tao, D. Taneja, M. H. Alam and D. Akinwande, *Chemical Society Reviews*, 2018, **47**, 6370-6387.
53. D. Y. Zubarev and A. I. Boldyrev, *Physical Chemistry Chemical Physics*, 2008, **10**, 5207-5217.
54. B. B. Averkiev, D. Y. Zubarev, L.-M. Wang, W. Huang, L.-S. Wang and A. I. Boldyrev, *Journal of the American Chemical Society*, 2008, **130**, 9248-9250.
55. B. L. Chen, W. G. Sun, X. Y. Kuang, C. Lu, X. X. Xia, H. X. Shi and G. Maroulis, *Inorganic Chemistry*, 2018, **57**, 343-350.
56. B. Chen, W. Sun, X. Kuang, C. Lu, X. Xia, H. Shi and G. L. Gutsev, *Physical Chemistry Chemical Physics*, 2018, **20**, 30376-30383.
57. B. Chen, G. L. Gutsev, D. Li and K. Ding, *Inorganic Chemistry*, 2022, **61**, 7890-7896.
58. Y. Tian, D. Wei, Y. Jin, J. Barroso, C. Lu and G. Merino, *Physical Chemistry Chemical Physics*, 2019, **21**, 6935-6941.
59. G. Frison and A. Sevin, *The Journal of Physical Chemistry A*, 1999, **103**, 10998-11003.
60. O. Tutusaus, R. Mohtadi, T. S. Arthur, F. Mizuno, E. G. Nelson and Y. V. Sevryugina, *Angewandte Chemie International Edition*, 2015, **54**, 7900-7904.
61. W. S. Tang, A. Unemoto, W. Zhou, V. Stavila, M. Matsuo, H. Wu, S.-i. Orimo and T. J. Udovic, *Energy & Environmental Science*, 2015, **8**, 3637-3645.